Soft Electronic Fluctuations in Sr_2RuO_4

M S Laad

Institute of Mathematical Sciences, Chennai, India

January, 2017

Collaborators

S Acharya (acharya.swagata@phy.iitkgp.ernet.in, IIT KGP, INDIA)

A Taraphder (arghya@phy.iitkgp.ernet.in, IIT KGP, INDIA)

D Dey (dibyendu.bkp@gmail.com, IIT KGP, INDIA)

T Mitra (tulika.maitra@gmail.com IIT R, INDIA)

Phase diagram for the iso-electronic series $Ca_{2-x}Sr_xRuO_4$

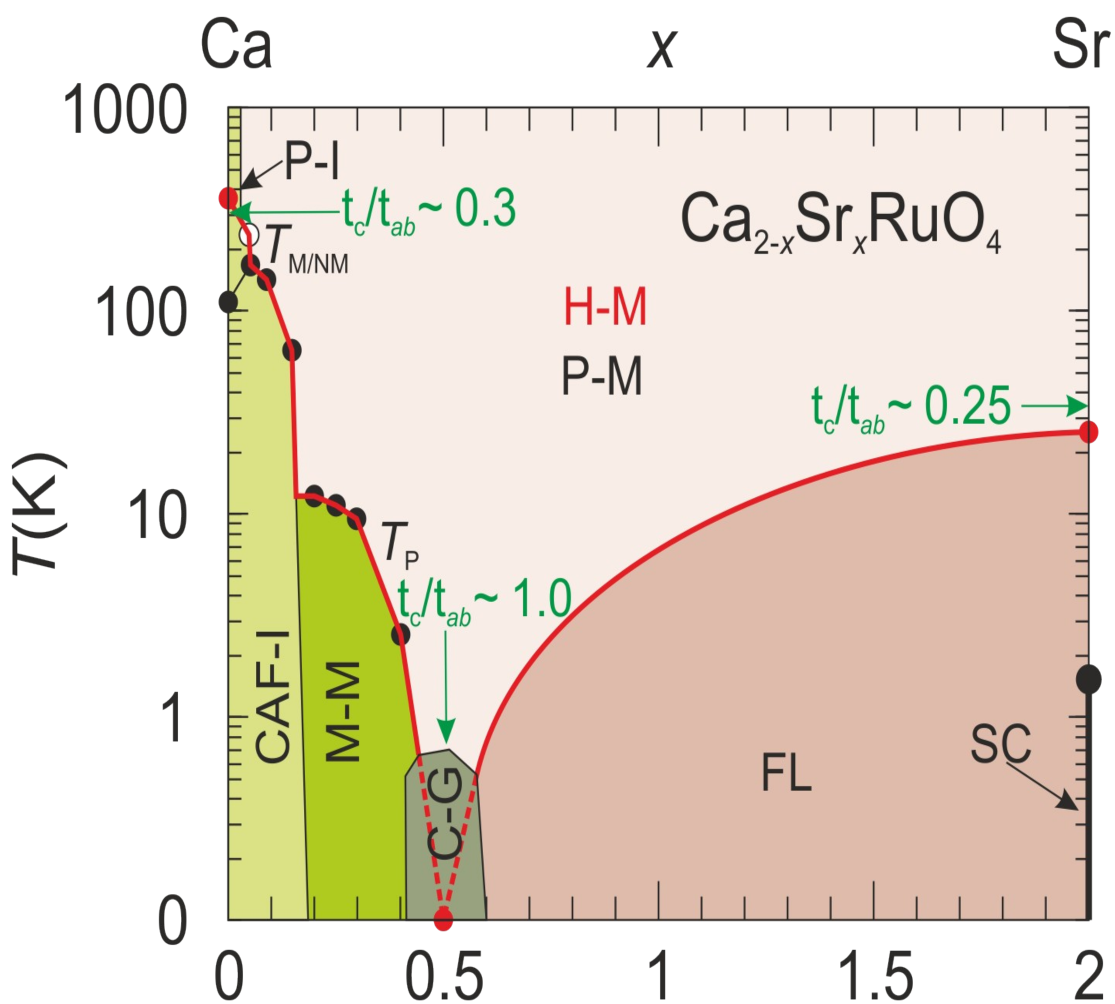

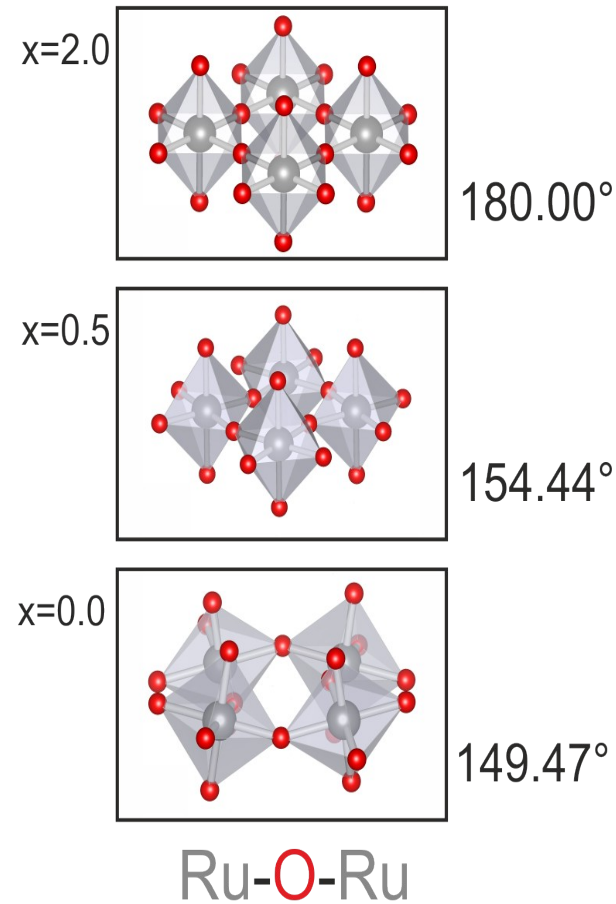

arXiv: 1605.05215

Outstanding Questions for Sr_2RuO_4

1. Retrieval of coherence scale (~ 25 K) in Normal Phase

2. Correlated metal, incoherent-coherent crossover.
   Fluctuations in the normal phase.

3. Role of SO coupling

4. Nature of the pairing wave function that leads to superconductivity: Experimental constraints.

Y. Maeno et al., (1994, 1998, 2001, 2004), Nakatsuji et al., (2003)

Crystal Structure

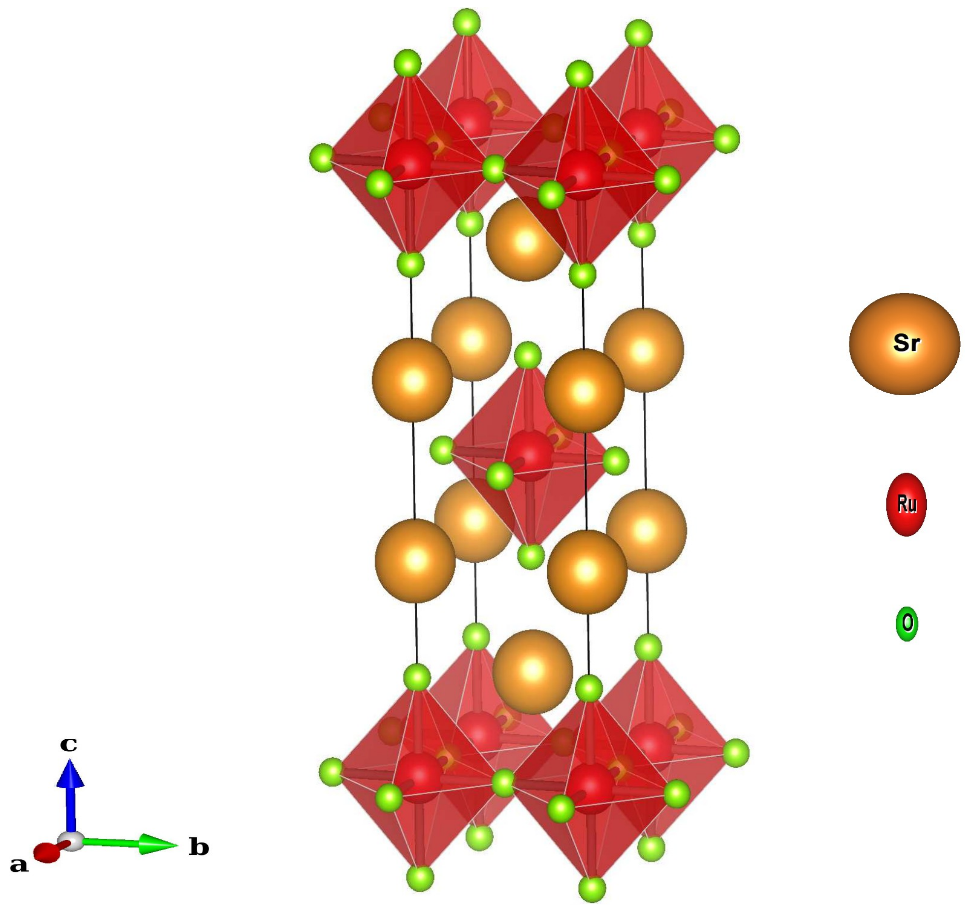

I4/mmm 139

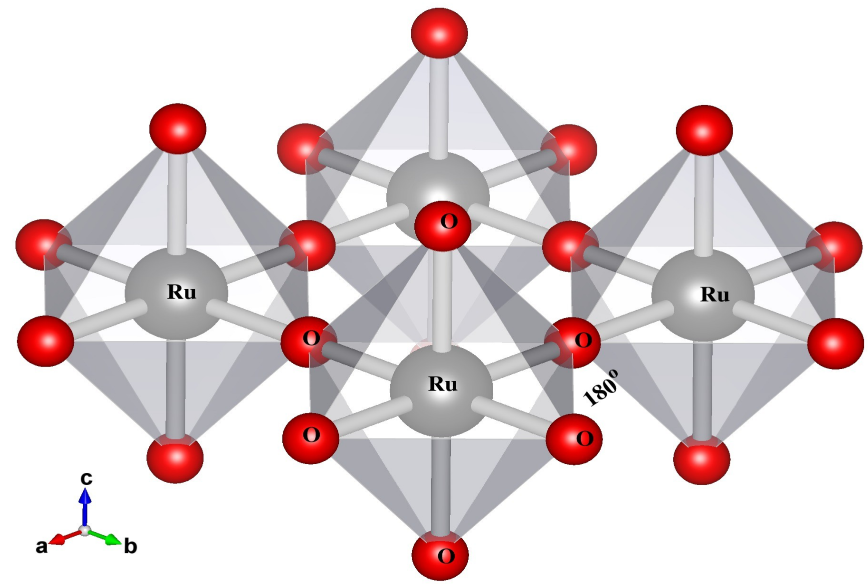

Ru-O-Ru 180^0

Experimental Motivations

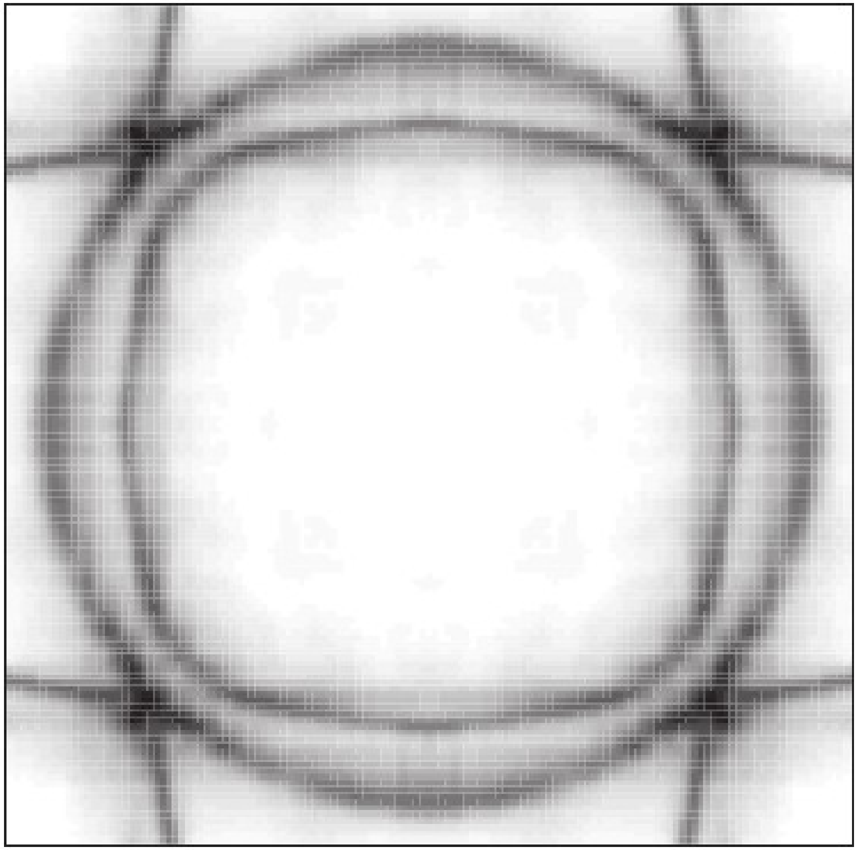

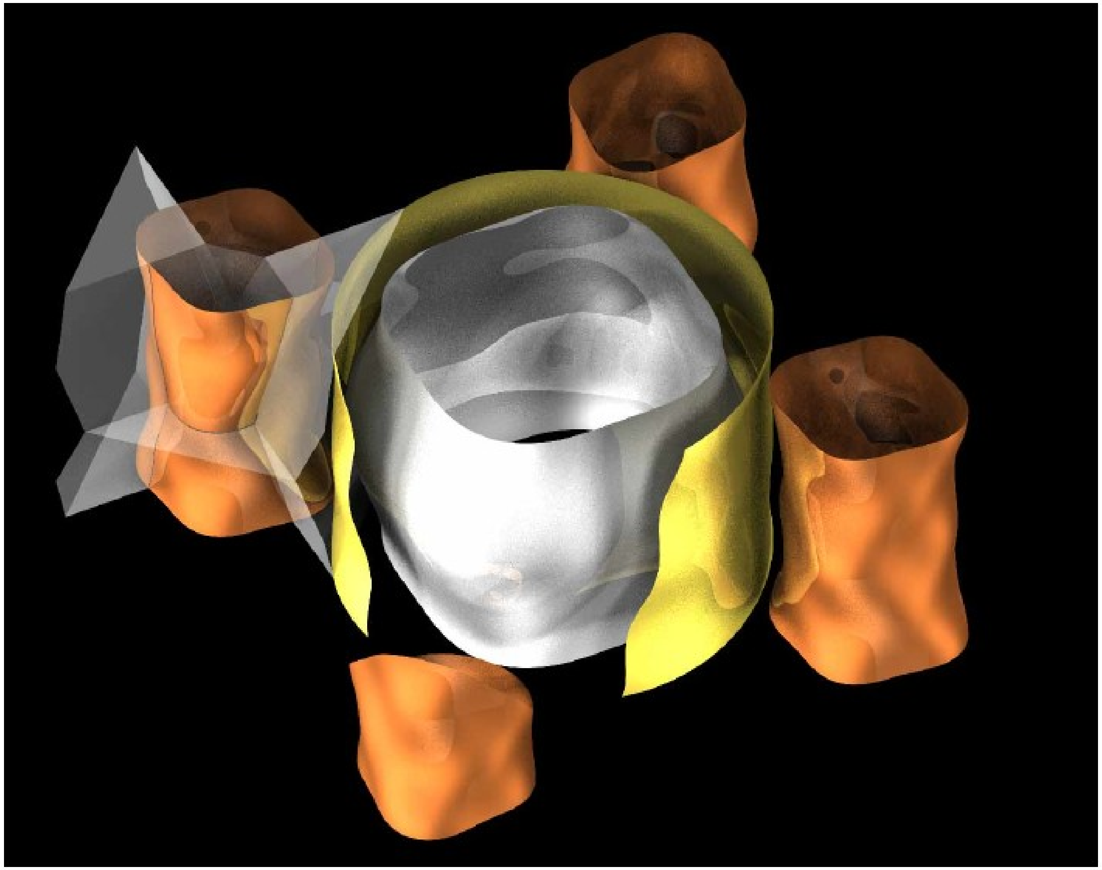

In-plane Fermi contour obtained from an ARPES F intensity map.

Visualization of the Fermi surface of Sr2RuO4. The c-axis corrugation is
exaggerated by a factor of 15 for clarity

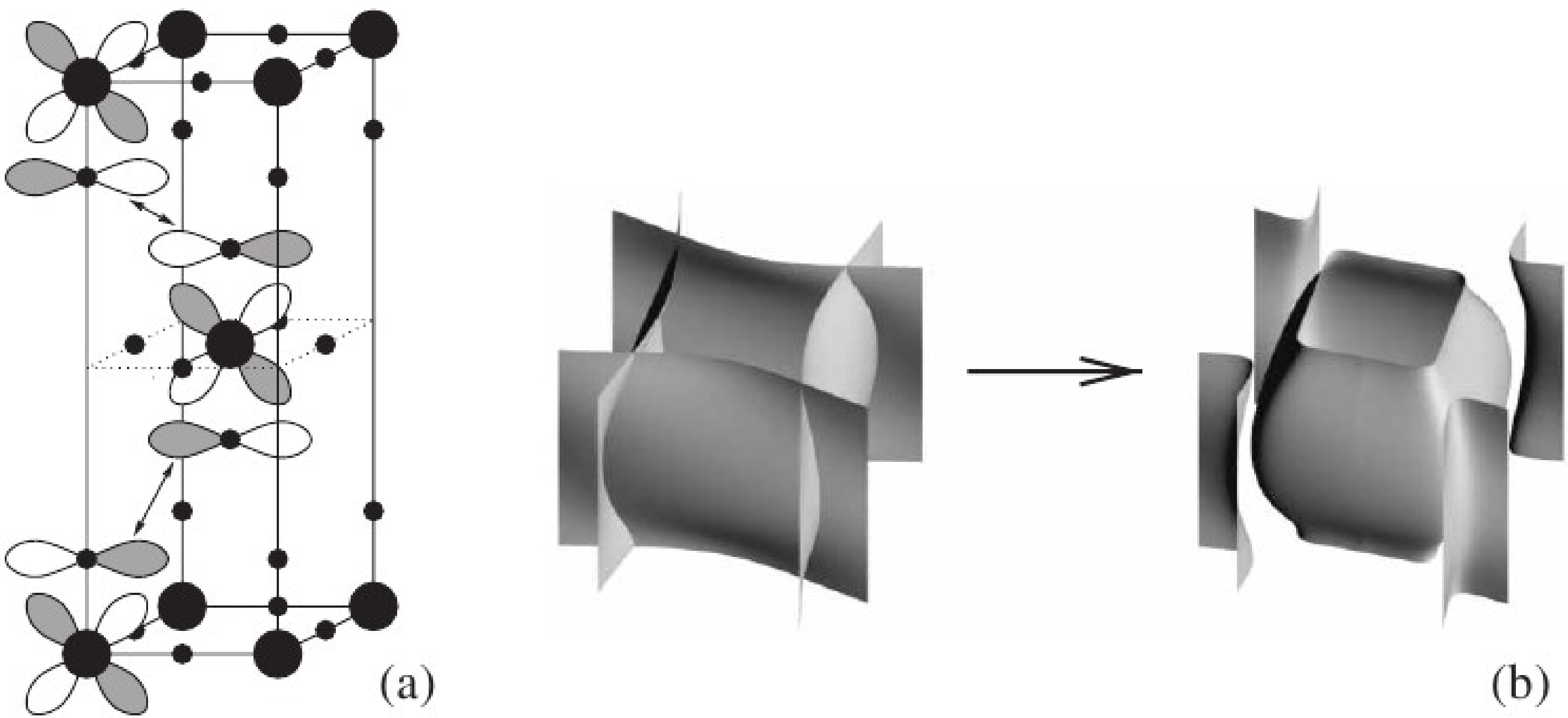

dxz=yz interplane overlap and warping of the
 and b sheets. (a) The dxz orbitals
in the crystal structure of Sr2RuO4 overlap along the c-axis, with positive overlap for
kz 1⁄4 0. Only the ruthenium and oxygen sites and only the relevant Ru 4dxz and O 2px
orbitals are shown. (b) The resulting corrugation of the quasi-1D Fermi walls (left)
translates into k21 -warping on the
 sheet and k01 -warping on the b sheet (right) when

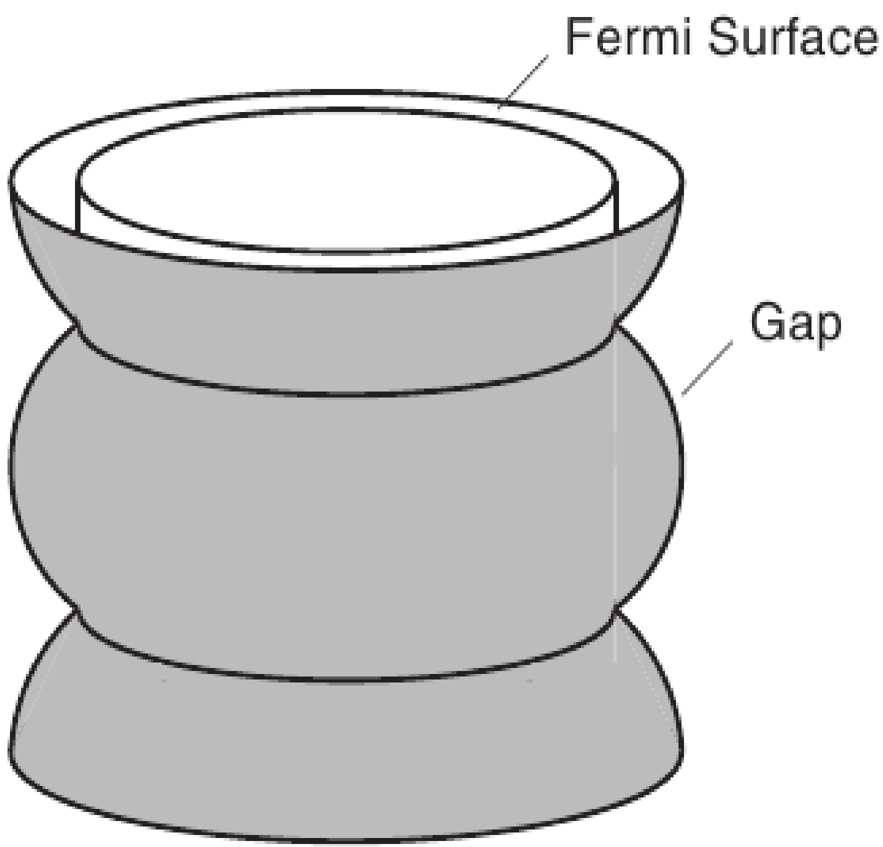

$$\frac{[t''_{\perp} \cos(ck_z/2)]^2}{[\epsilon_{\gamma}(\boldsymbol{k}) - \epsilon_{\alpha,\beta}(\boldsymbol{k})]}$$

Visualization of the gap function in equation (46) for a Fermi cylinder centred on À. The nodes are at kz 1⁄4 Æp=c, i.e. at Æ1=4 of the Brillouin zone height. The complex phase of the gap function rotates by 2p around the Fermi surface, as needed for a time-reversal symmetry-breaking superconductor.

Optical Conductivity

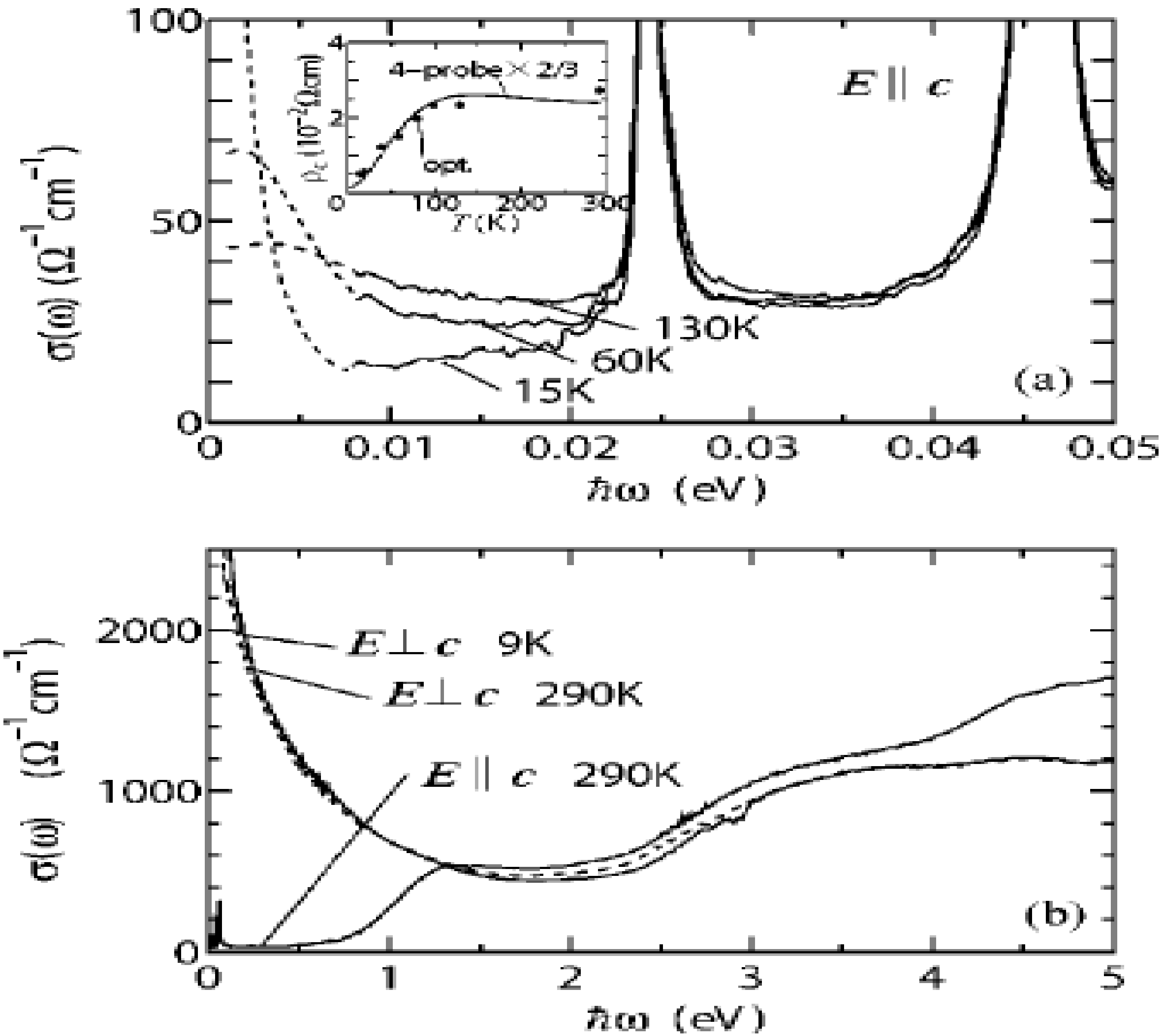

Resistivity

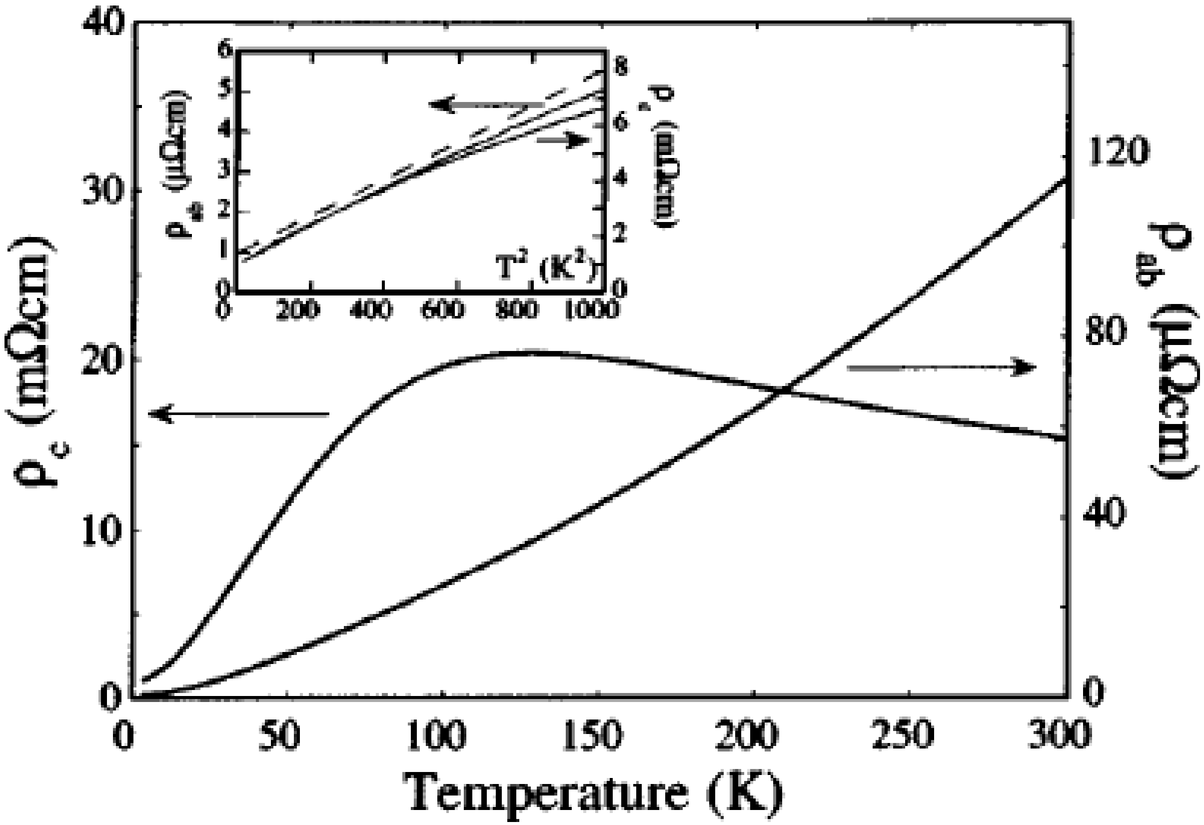

ω/T-scaling: Inelastic Neutron Scattering (Braden et al. 2002)

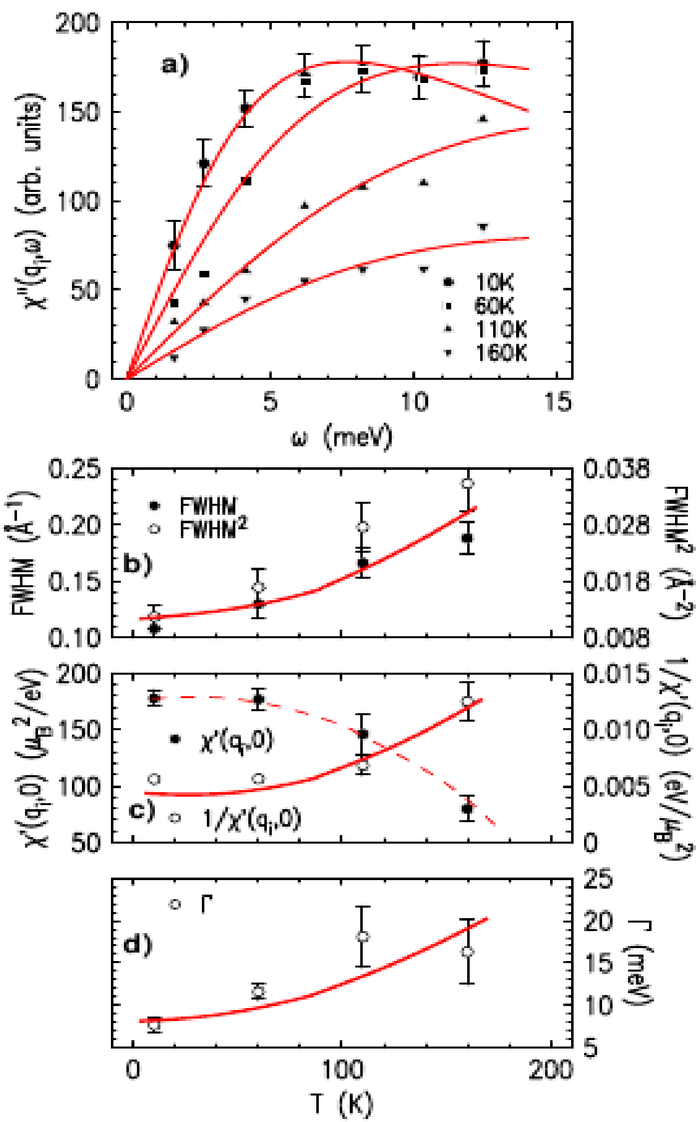

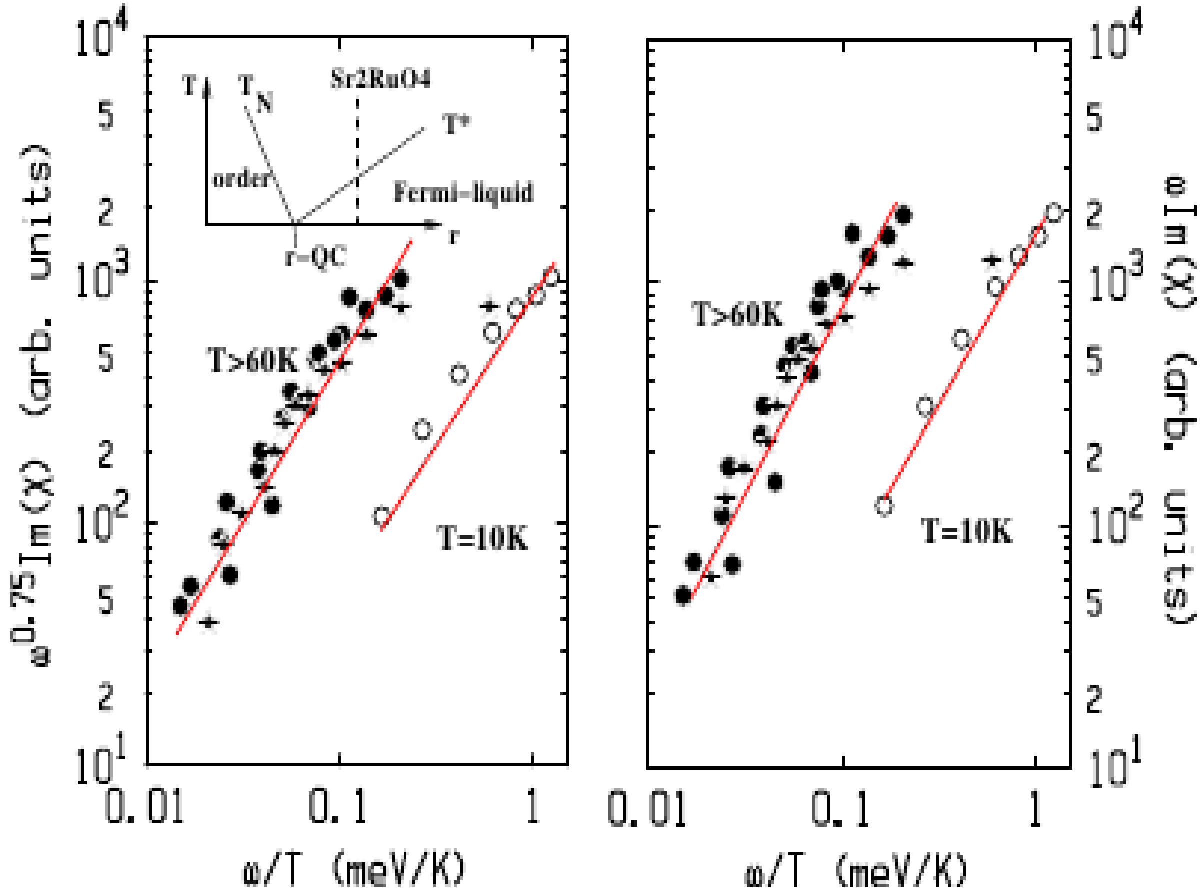

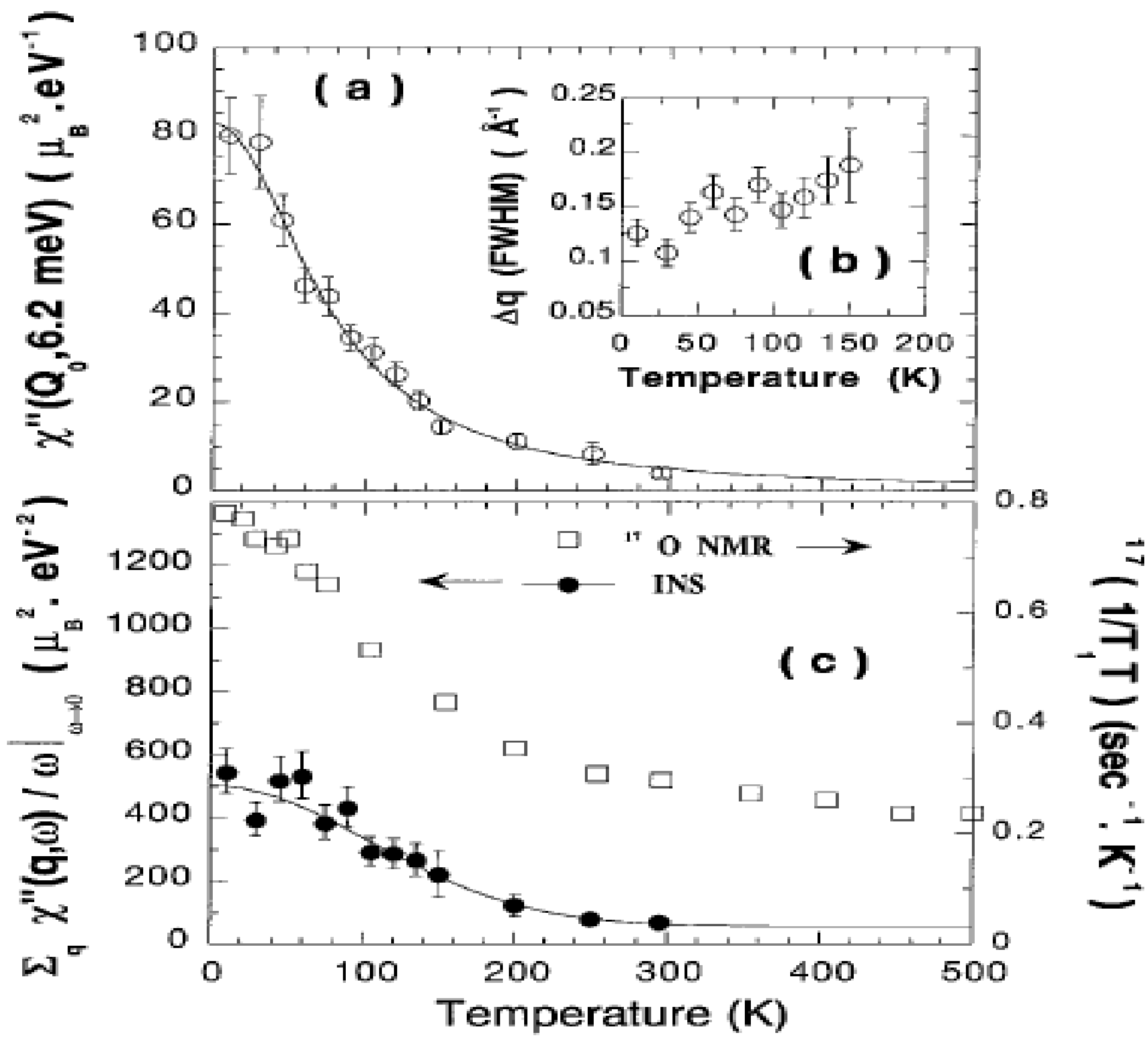

Results from fits to a Gaussian profile of 6.2 meV constant-v scans at Q0 ˓1.3, 0.3, 0̊ along the˓0, 1, 0̊: temperature dependences of (a) x 00˓Q0 , 6.2 meV˚ and (b) the intrinsic q width of the magnetic signal, Dq (FWHM). (c) Comparison between 17˓1T1 T̊ observed by 17 O NMR by Imai et al. [4] ( ) and the incommensurate contribution calculated from our INS measurements (≤). Assuming L 33 kOemB [25], the two scales in this figure are identical. Solid lines are guides to the eye only.

UNCONVENTIONAL SUPERCONDUCTOR!

Knight shift measurements and, recently, proximity-induced superconductivity in epitaxial ferromagnetic SrRuO3 layers provide strong evidence for triplet pairing.

Muon spin rotation and Kerr rotation experiments point to time reversal symmetry breaking at Tc , and tunneling spectroscopy to chiral edge states.

Spin-Orbital Entanglement

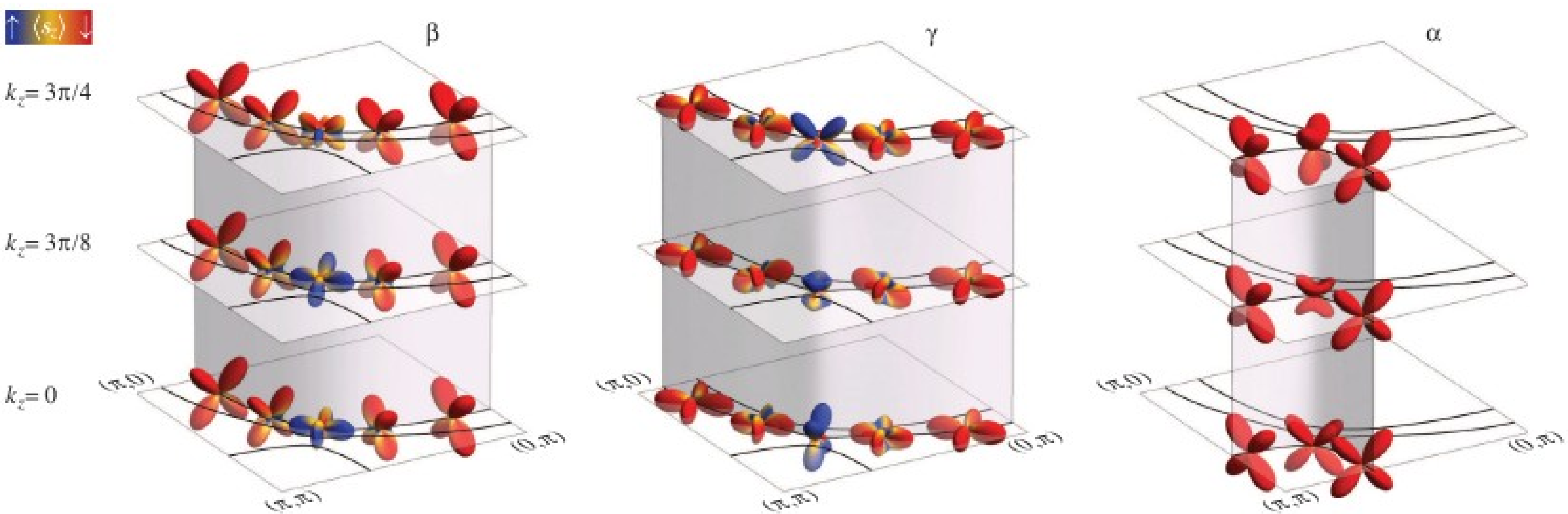

FIG. 3 (color online). Momentum-dependent Ru-d orbital projection of the wave function for the β, γ, and α bands at selected momentum locations along the three-dimensional Fermi surface. The surface color represents the momentum-dependent s_z expectation value along the direction defined by the spherical (θ, ϕ) angles, $\langle s_z \rangle_{(\theta,\phi)}$ [24]; as indicated by the color scale at upper left, blue/red correspond to spin $\uparrow/\downarrow$ for one state of the Kramers-degenerate pair (with the opposite spin state not shown [30]). The strongly mixed colors on some of the orbital projection surfaces for the β and γ bands indicate strong, momentum-dependent spin–orbital entanglement.

Damascelli et al. (Spin-polarized ARPES), 2014.

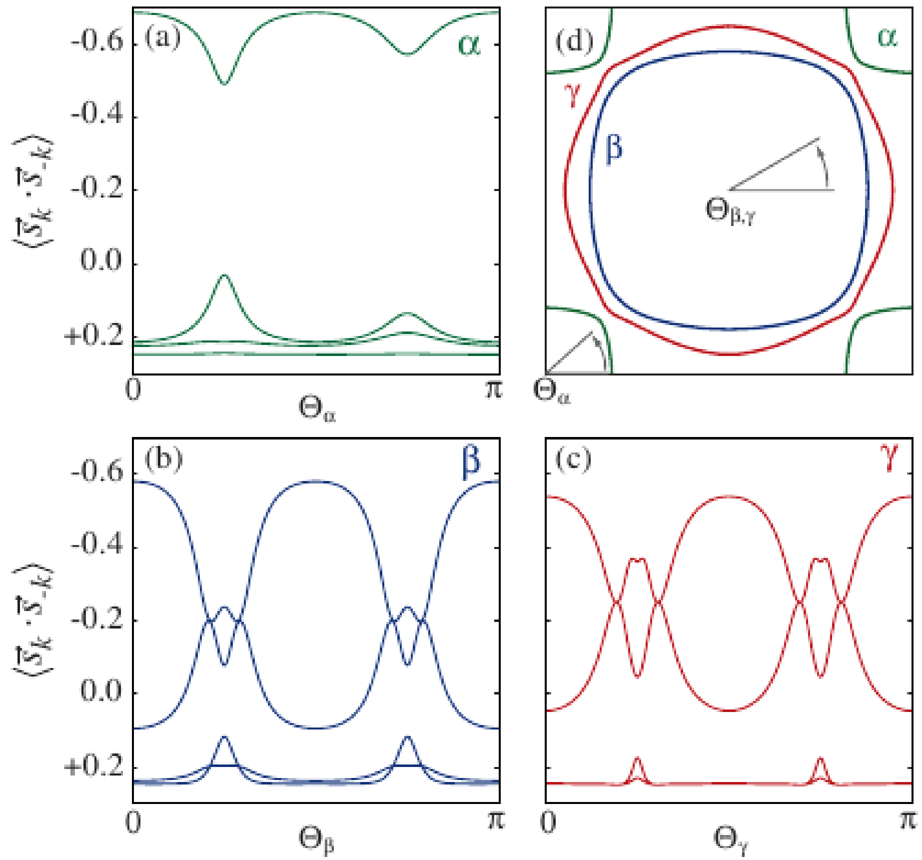

FIG. 4 (color online). Calculated two-particle spin expectation value $\langle s_{\vec{k}} \cdot s_{-\vec{k}} \rangle$ for states with zero total momentum along the $k_z = 0$ Fermi surface sheets for (a) α, (b) β, and (c) γ bands. The k_x–k_y plane location is defined by the angle Θ for each band, as illustrated in (d). The complete set of results for the full k_z range is shown in Fig. 5S of the Supplemental Material [24].

Strain Effects on the SC: Change in SC Pair Symmetry?

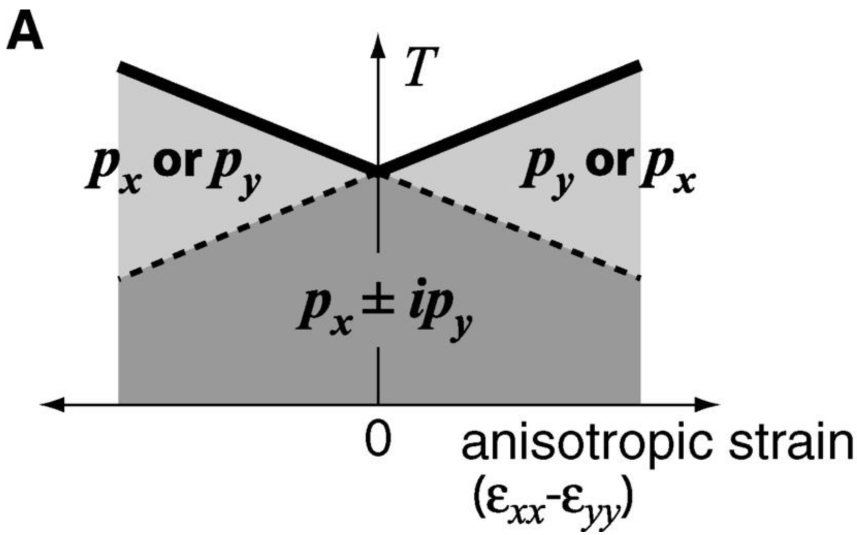

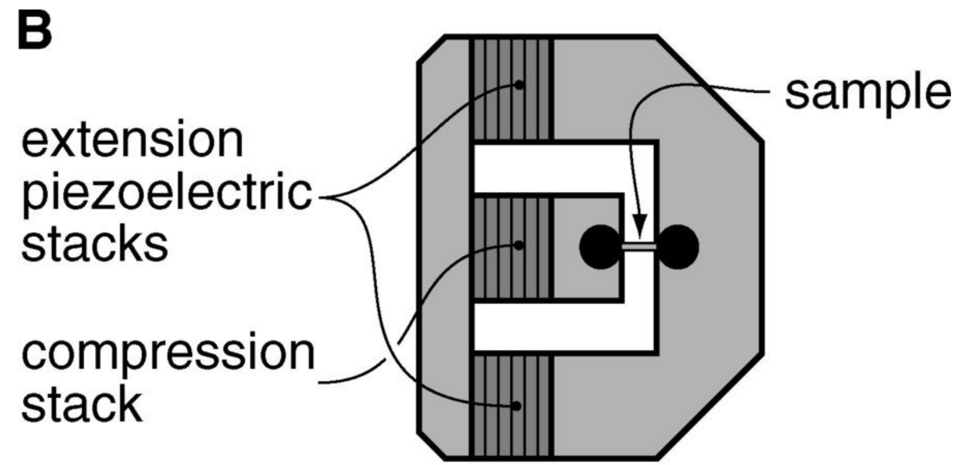

Strain Effects on SC: Pomeranchuk-like deformation of xy-FS sheet.

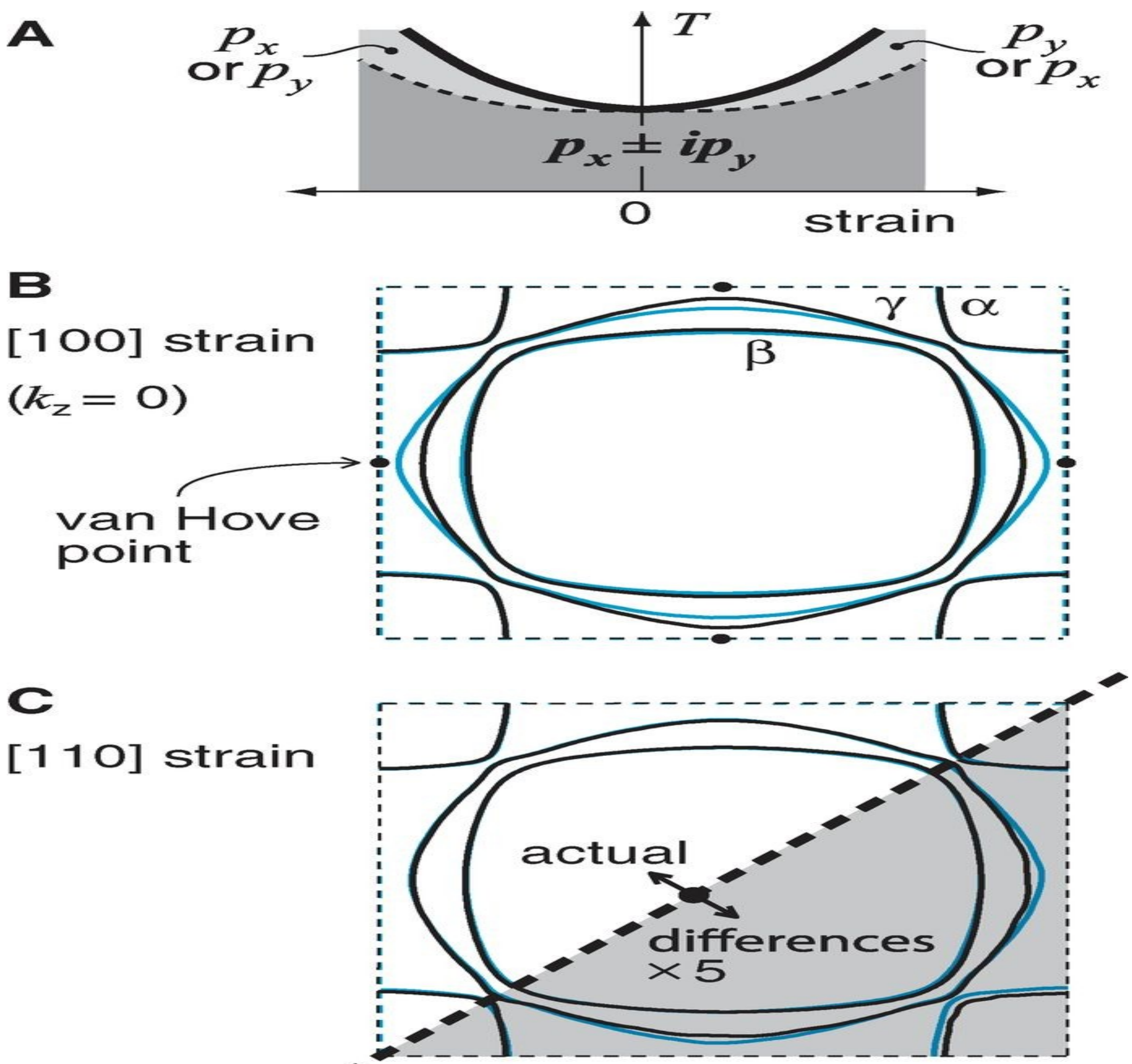

Wien2k and Wien2Wannier: spin-orbit entangled band states.

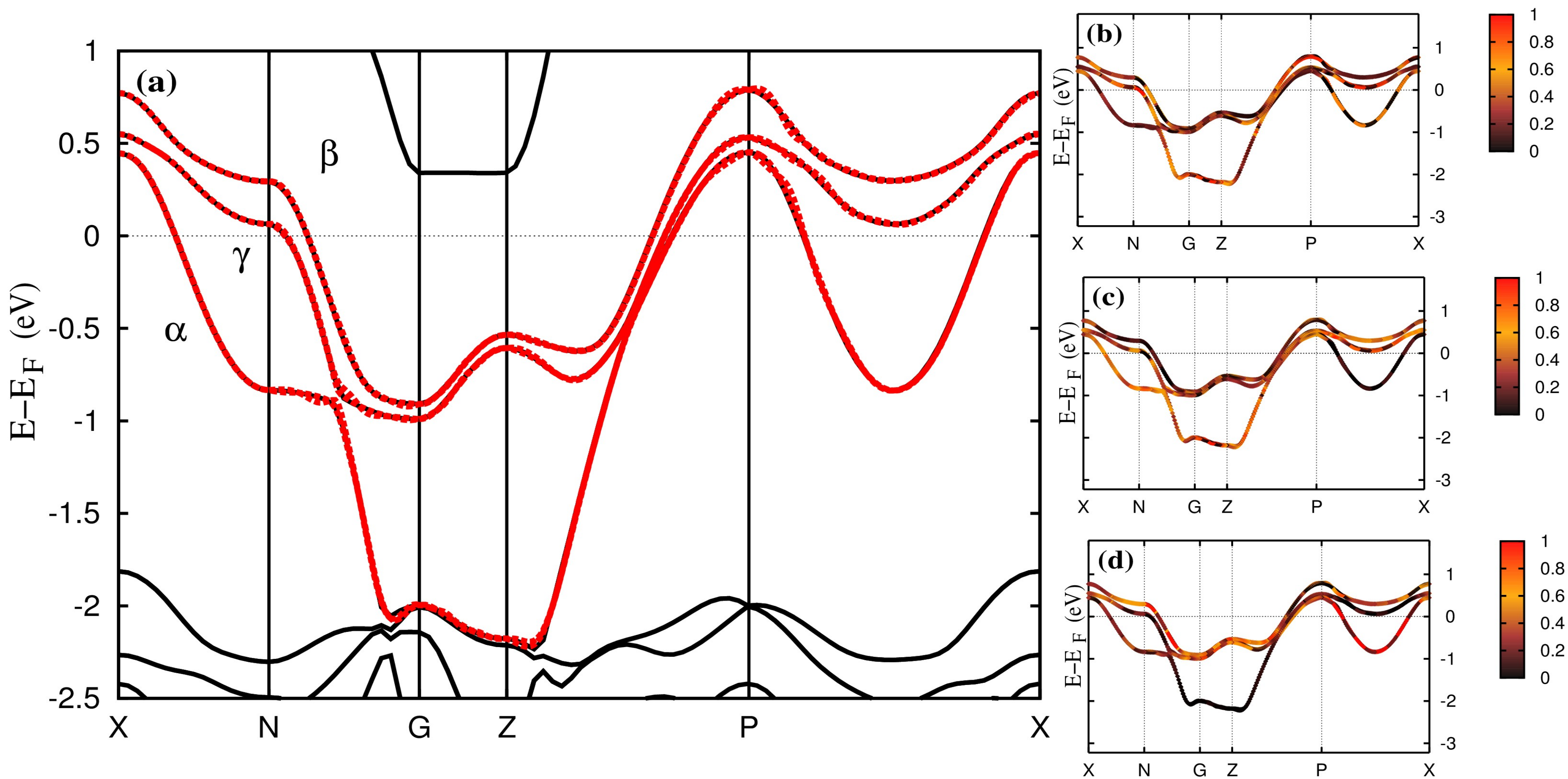

GGA+CT-QMC + DMFT

Experiments force a multi-orbital Hubbard model with intermediate-coupling.

Hubbard “U” comparable to LDA band width, “W”,

AND sizable SOC.

A 3 orbital CT-QMC + DMFT

(With and Without SO coupling)

Hamiltonian Formulation

$$H = H_{LDA} + H_{loc} - H_{dc}$$

where $H_{LDA} = \sum_{<i,j>} \sum_{\sigma,\sigma'} \sum_{a,b} c^{\dagger}_{ia\sigma} c_{jb\sigma'}$, $c^{\dagger}_{ia\sigma}$ creates an electron in a Wannier state in orbital a with spin-σ, etc, H_{dc} is the double-counting correction, and the $t^{ij}_{a\sigma,b\sigma'}$ are the hopping integrals ($i \neq j$) and on-site ($i = j$) *including* the SOC term? . H_{loc} describes the direct (with $U_{ab,ab} = U_{ab} = U - 2J(1 - \delta_{ab})$), exchange (with $U_{ab,ba} = J$), pair-hopping (with $U_{aa,bb} = J$) and spin-flip (with $U_{ab,ba} = J$) terms in the onsite t_{2g} basis. In the D_{4h} site symmetry, the t_{2g} states split into a b_{2g} singlet (xy) and e_g doublet (xz,yz), with $\epsilon_{xz} - \epsilon_{xy} = E_{cf} \simeq 120$ meV being the crystal field split-

Choice of U and J_H

$U = 2.3$ eV

$J_H = 0.4$ eV

↓

Correct orbital specific
quasi particle weights

GGA+SO+DMFT: Fermi Surfaces

Atomic SOC crucial!
(see also, Pavarini et al., 2016)

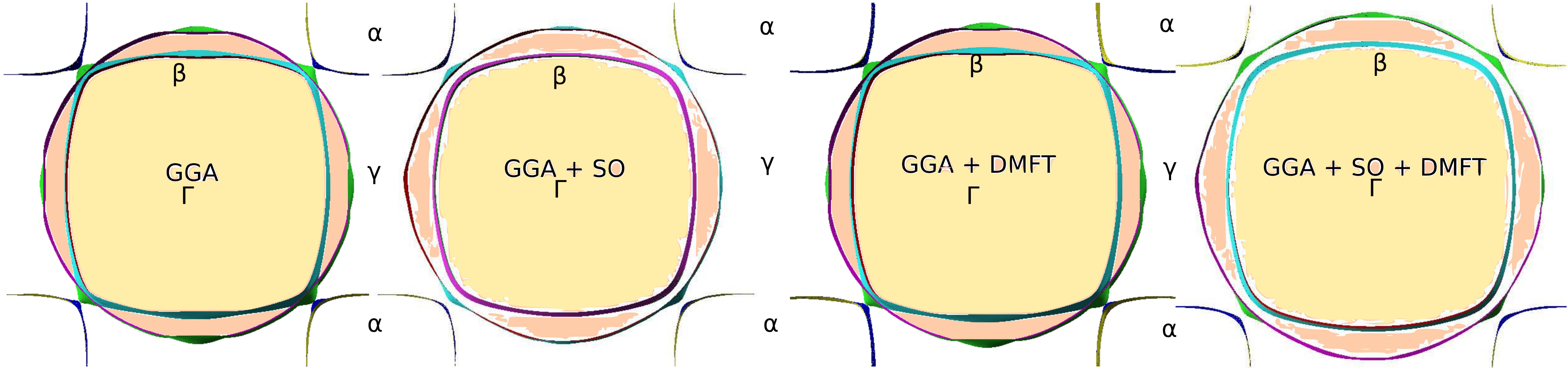

CT-QMC+ DMFT: Single and two particle responses

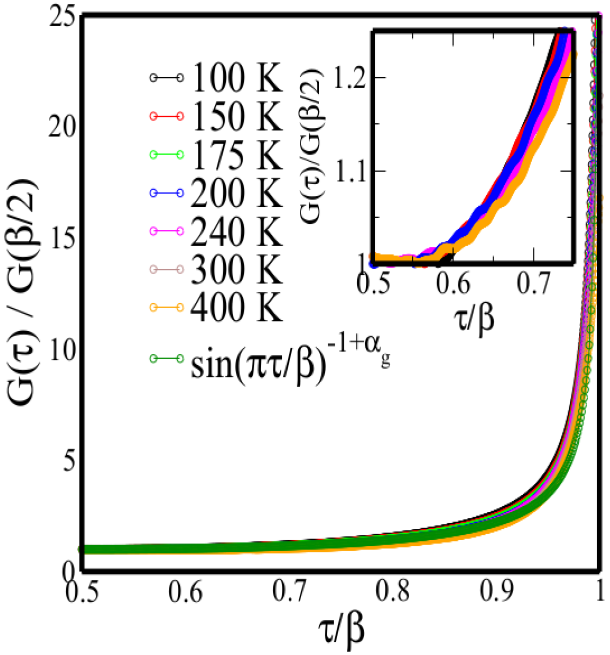

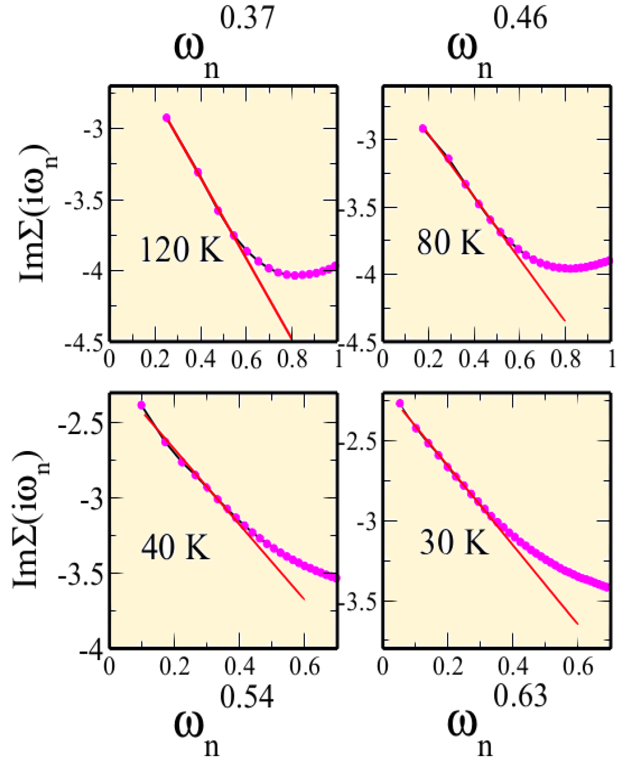

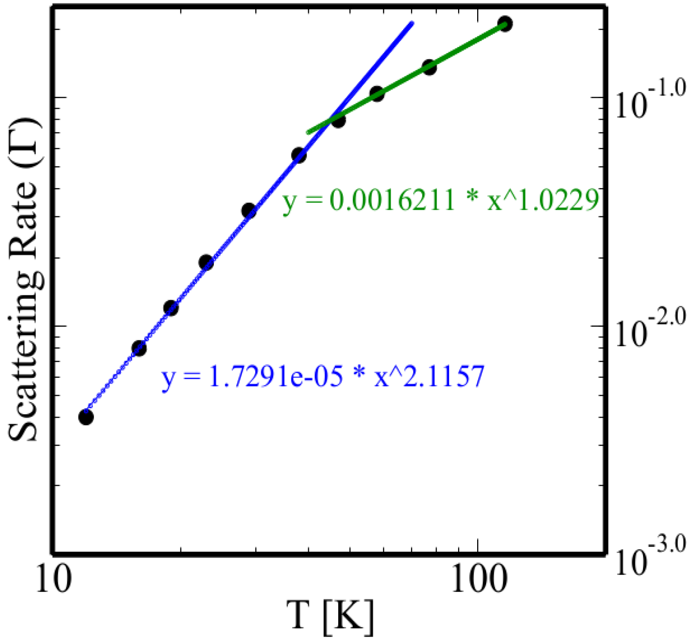

$T_{FL} \sim 41$ K

Scaling for Two-Particle Quantities: E/T-scaling for T>40K.

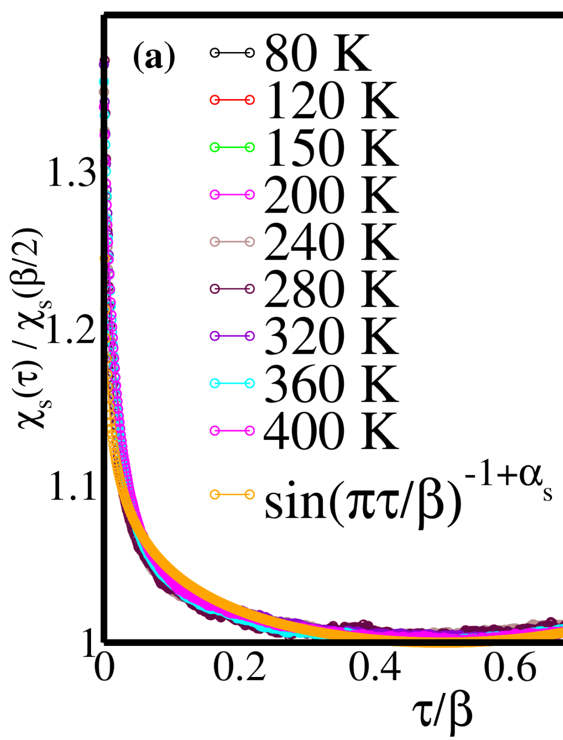

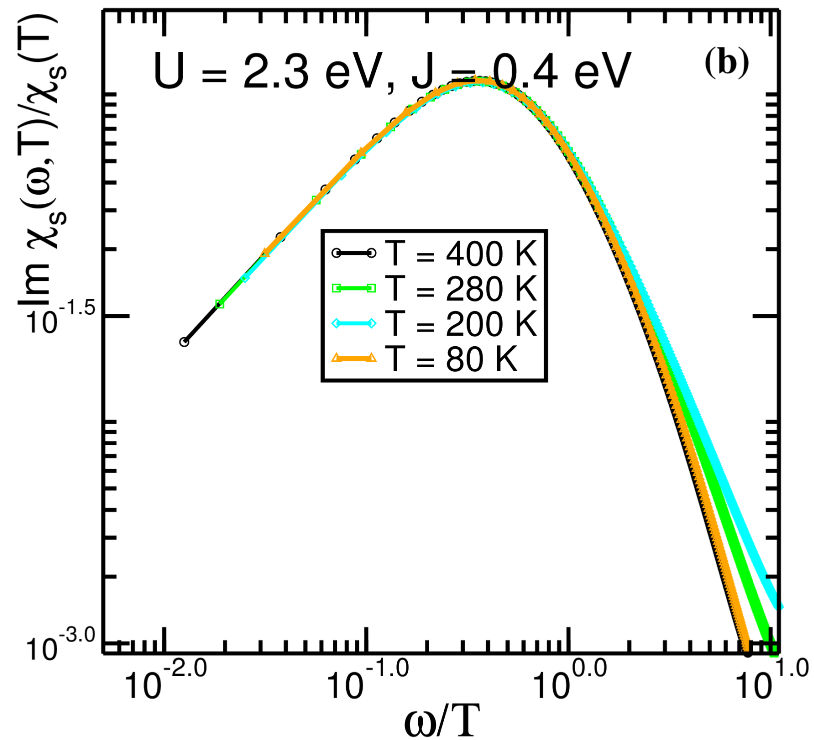

GGA+SO+CT-QMC+DMFT: Two particle responses

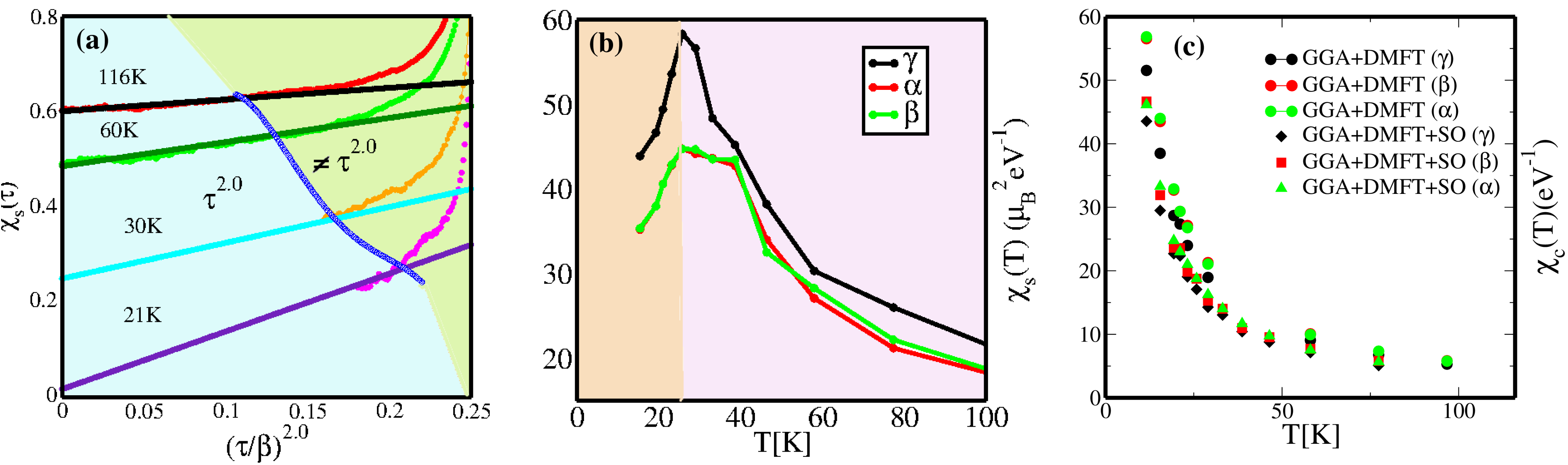

$T_{FL} \sim 23$ K

Aspect of Dimensional Crossover

$$H = \sum_{\nu} H_{1D}^{\nu} - \sum_{i,\nu,\nu',\sigma} t_{\perp}(C_{i\nu\sigma}^{\dagger} C_{i\nu'\sigma} + h.c)$$

where $\nu, \nu' = xz, yz$. A description of the crossover by perturbation theory in $t_{\perp}$ in the non-FL metal is beset with difficulties, and is valid only in the non-FL regime, but fails to reproduce the FL regime. Perturbation approaches in interaction, beginning from the free band structure work in the FL regime, but fail in the non-FL regime. An attractive way out is provided by generalization of a non-trivial argument developed in the context of coupled Luttinger chains[?] . In our case, each RuO_2 layer is connected via $t_{\perp}$ to $z_{\perp}$ nearest neighbors, with $z_{\perp} \to \infty$. Rigorously, one needs a numerical solution for the *full* local propagator, $G(k, \omega)$, which we take from our LDA+DMFT calculation (see main text). Using this input, we can draw qualitative conclusions regarding the effect of non-FL metallicity at high-T on the non-FL to FL crossover at lower T as follows. In the non-FL regime, for each of the quasi-1D xz,yz bands, the in-plane self-energy $\Sigma_{\nu}(\omega) \simeq (t(\omega)/t)^{1/(1-\alpha)}$[?] . It is clear that $t_{\perp}$ becomes relevant, inducing the dimensional crossover when $t_{\perp}^{\nu\nu'} > \Sigma_{\nu}$, yielding the crossover scale $E^{*} \simeq t_{\perp}(t_{\perp}/t)^{\alpha/(1-\alpha)}$. With $\alpha = 0.32$ in our case, this yields $E^{*} \simeq 40$ K, in good accord with the numerical estimate of 23 K in the main text.

Aspects of Dimensional Crossover

Once $T < E^*$, one ends up with an anisotropic correlated FL metal. In particular, when $t_\perp << t$ and at low energies, all one-particle quantities obey the scaling $\omega' = \omega/E^*$, and $T' = T/E^*$; i.e., $t\Sigma(\omega, T) = E^* t_\perp \Sigma'(\omega', T')$ and $tG(\omega, T) = (E^*/t_\perp)G'(\omega', T')$ where Σ and G are universal functions associated with the crossover. A low-frequency expansion of Σ in the FL regime gives the quasiparticle residue $Z \simeq (t_\perp/t)^{\alpha/(1-\alpha)} = E^*/t_\perp$. The inter-layer resistivity, $\rho_\perp(T)/\rho_0 = (t/E^*)R(T/E^*)$ with $R(x << 1) \propto x^2$ and $R(x >> 1) \propto x^{1-2\alpha}$. And the resistivity enhancement, $\rho_\perp(T)/\rho_0 = A(T/t)^2$ with $A = (t/t_\perp)^{3/(1-\alpha)}$. The resulting anisotropy of the Woods-Saxon ratio, $A_c/A_{ab} = (a/c)^2 A \simeq 1000$ for $\alpha = 0.32$, which is indeed in the right range[1]. Finally, the c-axis optical response is incoherent above E^*, with a coherent feature carrying a relative weight $\simeq Z^2$ appearing at low-T, again in qualitative agreement with observations[19] . An obvious inference from the above is that increasing T should lead to a disappearance of the quasicoherent features in photoemission. This may already have been observed experimentally[24].

NFL-FL Crossover

$$H = \sum_{\nu} H_{1D}^{\nu} - \sum_{i,\nu,\nu',\sigma} t_{\perp}(C_{i\nu\sigma}^{\dagger} C_{i\nu'\sigma} + h.c)$$

The physical mechanism for this crossover (which is also a dimensional crossover) is the increasing relevance of the inter-layer one-electron hopping at lower
T , since the SOC seems to become relevant at higher T as reflected in the in-plane versus out-of-plane spin susceptibility anisotropy? .

Single and Two-particle scaling Features

A proper thermal scaling collapse for both the the field propagators

The thermal scaling feature is violated below ~ 23 K

Below ~23 K there is dominant Fermi liquid like scalings in both single and two particle sectors.

Soft Charge Fluctuations

<u>Charge fluctuations</u> are <u>softer</u> than spin flcutuations down to lowest tempearture.

Raghu et al., 2013 J. Phys.: Conf. Ser. 449 01203

Raghu and Kivelson, Phys. Rev. Lett. 105 (2010), 136401.

Alexander Steppke et al., April 2016 arXiv. 1604.06669

Pairing

Multi-band spin-triplet and odd-parity pair state with form factor

$$\mathbf{\Delta}(\mathbf{k}) = \mathbf{z}\Delta_0(sin\frac{k_x a}{2}cos\frac{k_y a}{2}+icos\frac{k_[x}{a}2sin\frac{k_y a}{2}).(cos\frac{k_z c}{2}+a_0)$$

which reduces to the form $\mathbf{\Delta}(\mathbf{k}) = \mathbf{z}\Delta_0(k_x + ik_y)(cos(k_z c) + a_0)$ for small k_x, k_y, where the a_0 component can exist on symmetry grounds in Sr_2RuO_4? .

line nodes at $k_z = \pm\pi/2c$ as long as $|a_0| < 1$

References

1. S. Acharya et al., to be published in Nature: Scientific Reports (arXiv:1605.05215v1 (2016)).

2. J Mravlje et al., arXiv. 1010.5910v2 (2010).

3. X. Deng et al., arXiv. 1504.00292v1 (2015).

4. J Mravlje, A Georges 1504.03860v1 (2015).

Thank You

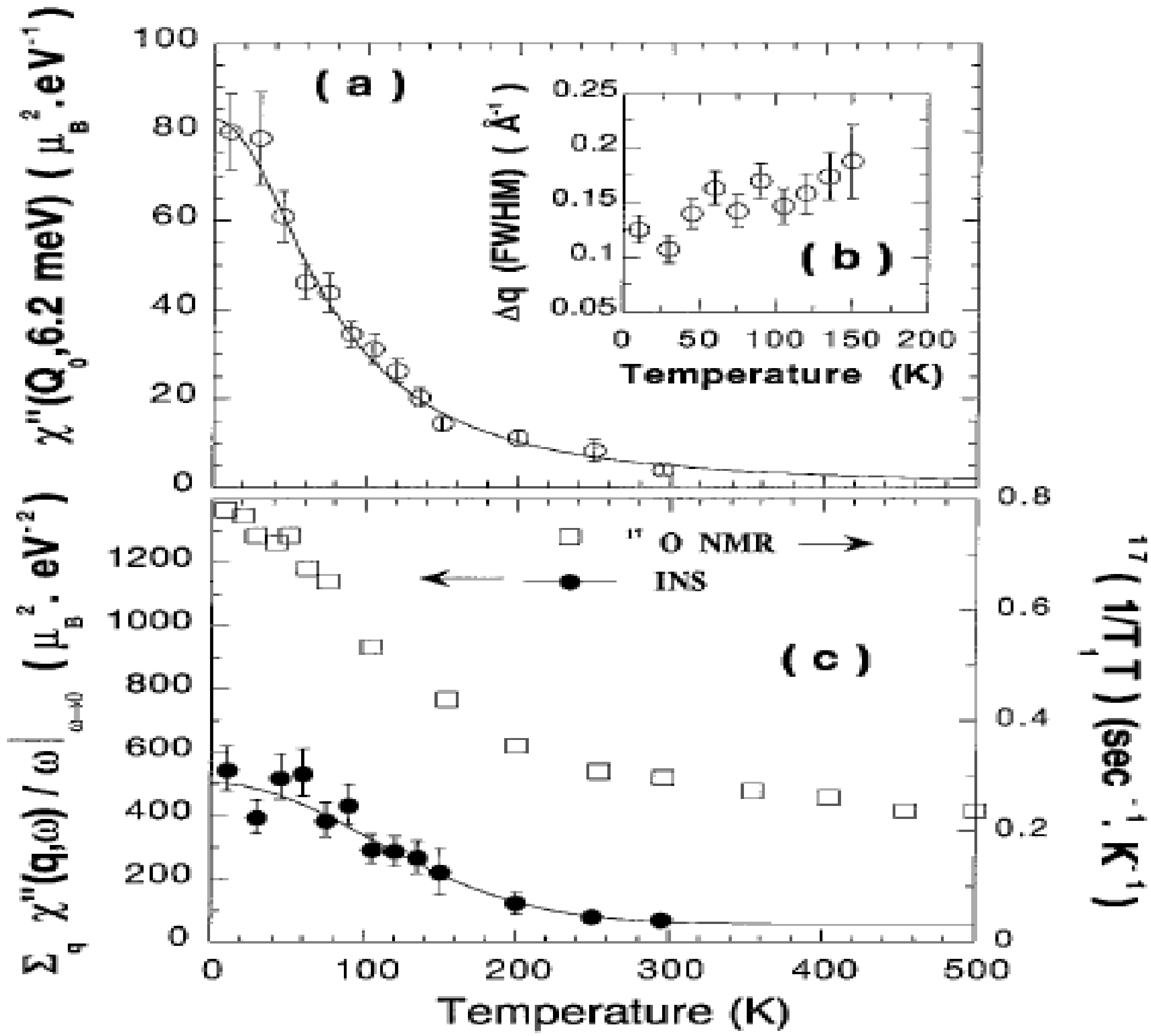

Results from fits to a Gaussian profile of 6.2 meV constant-v scans at Q0 ʿ1.3, 0.3, 0̂ along theʿ0, 1, 0̂: temperature dependences of (a) x 00ʿQ0 , 6.2 meV̂ and (b) the intrinsic q width of the magnetic signal, Dq (FWHM). (c) Comparison between 17ʿ1T1 T̂ observed by 17 O NMR by Imai et al. [4] ( ) and the incommensurate contribution calculated from our INS measurements (≤). Assuming L 33 kOemB [25], the two scales in this figure are identical. Solid lines are guides to the eye only.